J. Electrochem. Sci. Eng. **9(2)** (2019) 85-97; http://dx.doi.org/10.5599/jese.624

Open Access: ISSN 1847-9286
https://pub.iapchem.org/ojs/index.php/JESE

Original scientific paper

Comparative study of Al_2O_3, SiO_2 and TiO_2-coated $LiNi_{0.6}Co_{0.2}Mn_{0.2}O_2$ electrode prepared by hydrolysis coating technology

Daxian Zuo[1], Cuiping Wang[1], Guanglei Tian[2], Kangying Shu[2], Xingjun Liu[1,3,✉]

[1]*College of Materials and Fujian Provincial Key Laboratory of Materials Genome, Xiamen University, Xiamen, 361005, P. R. China*
[2]*College of Material Science and Engineering, China Jiliang University, Hangzhou, 310018, P. R. China*
[3]*Department of Materials Science and Engineering, Harbin Institute of Technology, Shenzhen, Guangdong, 518055, P. R. China*

✉Corresponding author: lxj@xmu.edu.cn; Tel.: +86-592-2187888

Received: October 8, 2018; Revised: January 18, 2019; Accepted: January 19, 2019

Abstract

In this work, Al, Si and Ti oxides are used to modify the surface of $LiNi_{0.6}Co_{0.2}Mn_{0.2}O_2$ (NCM622) electrode through the hydrolysis coating technology. SEM and TEM results revealed that three prepared oxide layers have different uniformity and morphology. Also, charge-discharge results showed different initial discharge capacity and cycle ability of three different oxide coatings. It is shown that when the temperature is increased from 25 to 50 °C, the capacity retention of Al_2O_3-coated NCM622 is reduced by only 4 %, what demonstrated the best ability of this oxide to restrain cycle deterioration. Additionally, when the charge cutoff voltage is increased to 4.6 V, Al_2O_3-coated NCM622 showed 74 % of capacity retention. As the number of charge-discharge cycles increases, the dissolution of some transition metal ions may be restrained by Al_2O_3 layer. Generally, the enhanced electrochemical performance of Al_2O_3-coated NCM622 could be ascribed to the suppression of mutual reaction between electrode and electrolyte and improvement of structural stability of the material by Al_2O_3 coating.

Keywords

Lithium ion battery; nickel-rich layered cathode; oxide coating layer; electrochemical performance; polarization resistance

Introduction

In recent years, lithium ion batteries with high energy density have attracted much attention in the field of mobile devices such as notebook computers, cellular phones, and digital cameras [1-4]. Especially cathode materials play a key role in obtaining high energy density. Among them, the nickel-rich layered cathode materials, $LiNi_xCo_yM_{1-x-y}O_2$ (x>0.5) with α-$NaFeO_2$ structure [5-8], are considered as promising candidates to satisfy high capacity and rate capability criteria. For the nickel-rich layered cathode materials, however, although the discharge capacity would increase with amount of Ni^{2+}, formation of the hybrid between Ni^{2+} and Li^+ would result in a cycle decay [9,10]. Whereas at present improvement of the charge voltage may be a key research direction for cathode materials, it can generally be expected that significant increase of interfacial resistance between nickel-rich layered cathode materials and electrolyte [11] would also lead to rapid capacity decay. Additionally, the rate capability and cycle stability at elevated temperatures were found poor for this material [12]. All these drawbacks limit further application of nickel-rich layered cathode materials.

To resolve these problems, a lot of efforts have been made to ameliorate the surface structure of nickel-rich layered cathode materials by various approaches [13-15]. Thus, the surface coating has generally been recommended as a simple and effective technique to improve the rate capability and cycleability at elevated temperatures, inhibit cation dissolution into electrolyte and suppress the growth of polarization impedance [16,17]. Besides, the presence of the coating layer could also restrain the interfacial reaction between electrode and electrolyte, and protect the electrode material from the HF attack during the charge-discharge process [18,19]. Therefore, better performance is expected to be achieved by surface coating, even in conditions of higher upper limit voltage and increased temperature.

NCM622 is a representative kind of nickel-rich layered cathode materials with a high initial discharge capacity, approximately 200 mAh g^{-1} [20]. Unfortunately, just like other nickel-rich layered cathode materials, NCM622 showed many intrinsic drawbacks of $LiNiO_2$ [21], such as thermal instability and poor cycle stability. So far, the commercialized application of this cathode material has been inhibited by its severe capacity fading during high temperature and voltage cycling. To solve these problems, the surface coating has been proved to be an effective technology. Metal oxides such as Al_2O_3 [22], ZrO_2 [23], V_2O_5 [24], and ZnO [25] have been reported as very effective coating materials. It has already been shown [26-28] that for different oxide coating materials, the uniformity, thickness and structure characteristic of each coating layer are different, what would lead to different electrochemical performances. Therefore, it becomes necessary to make a comparative study of the relationship existing between each oxide coating layer and electrochemical behavior of the coated NCM622 electrode. Unfortunately, there are only few literature data on this aspect.

In this study, a commercial sample of NCM622 is coated with Al_2O_3, SiO_2 and TiO_2, by using the hydrolysis coating technology. Corresponding structures and electrochemical properties of NCM622 coated by these three oxides are examined, and the correlation between oxide coating layers and electrochemical performance of the coated NCM622 is discussed in detail.

Experimental

Sample preparation

Commercial NCM622 (Ningbo Jinhe New materials Co. , Ltd, China) was used as the pristine material. Aluminum isopropoxide (AIP), tetrabutyl titanate (TBT) and tetraethyl orthosilicate (TEOS)

were used as precursor reagents for the corresponding oxide coatings. Throughout this paper, pristine NCM622, Al_2O_3-coated NCM622, SiO_2-coated NCM622 and TiO_2-coated NCM622 are marked as P-NCM622, A-NCM622, S-NCM622 and T-NCM622, respectively. Since it was shown previously [17] that the cathode material with oxides and active material in the weight ratio of 1:99 has better electrochemical performance, in this work, the oxide-coated NCM622 materials with oxide and NCM622 in the same weight ratio (1:99) were synthesized by the hydrolysis coating technology. Figure 1 describes schematically the coating procedure.

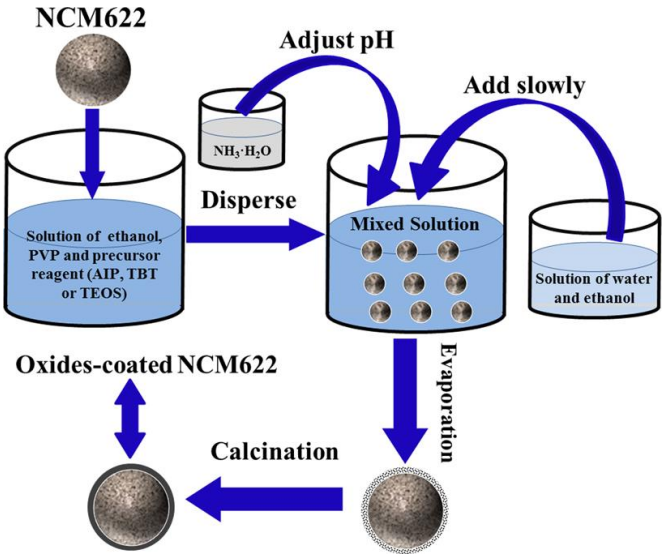

Figure 1. *Schematic illustration of oxide coating layer formation on NCM622.*

The stoichiometric amount of the precursor reagent was firstly dissolved in ethanol, and polyvinyl pyrrolidone (PVP, 0.8 g) was added into the solution. Then the NCM622 powder (39.6 g) was dispersed in the solution, and stirred at room temperature for 1 h. After that, 50 mL of distilled water/ethanol (volume ratio=1:9) was added to the mixed solution slowly during 1 h with vigorous stirring, and the solution pH value was adjusted to 10.0 by 0.1 M $NH_3 \times H_2O$ solution. The mixed solution was then continuously stirred at 60 °C until the solvent was evaporated. At last, the product was washed, dried and then treated at 600 °C for 4 h, giving the final sample. For comparison purpose, the pristine NCM622 sample was subjected to the same procedure, but without "active component" as aluminum, silica or titanium compounds.

Structure and morphology characterizations

Powder X-ray diffraction (XRD) data were collected using X-ray diffractometer (Thermo ARL, X' TRA) equipped with a Ni-filtered Cu-Kα radiation at 40 kV and 20 mA for structure analysis. Also, the diffraction patterns were recorded between scattering angles of 10 and 90° in steps of 0.02°. The surface morphology of all samples was observed using a scanning electron microscope (SEM, HITACHI SU8010) and transmission electron microscope (TEM, JEOL JEM 2100). Additionally, the electron diffraction spectroscopy (EDS) mapping was examined to confirm the surface element distribution, together with SEM in a large field of view.

Electrochemical characterizations

Electrochemical performances of all samples were examined using CR2430-type coin cells. A metallic lithium foil was used as the negative electrode. The positive electrodes were prepared by mixing 90 wt% of active material (commercial NCM622 particles or as-prepared oxides-coated NCM622), 5 wt% of acetylene black conductive additive, 5 wt% of polyvinylidene fluoride (PVDF)

binding agent and proper amount of N-methyl-2-pyrrolidone (NMP) solvent to form the slurry. The as-prepared black slurry was pasted on the current collector (aluminum foil) and followed by drying at 90 °C in a vacuum oven overnight. Electrodes were cut into small wafers with diameter of 16 mm. The active material surface loadings on Al foils were about 7-8 mg cm^{-2}. The electrolyte solution consisted of 1 mol dm^{-3} $LiPF_6$ dissolved in ethylene carbonate (EC)/dimethyl carbonate (DMC) (1:1, v/v). A polypropylene microporous film (Cellgard 2300) was used as a separator. The cells (CR 2430) were assembled in an argon-filled glove box with water/oxygen content less than 0.1 ppm (Super 1220/750, MIKROUNA). Galvanostatic electrochemical test data were collected on a multi-channel battery cycler (CT2001A, Wuhan LAND Electronic Co. , Ltd) at different temperatures. The impedance spectroscopy (EIS) and cyclic voltammogram (CV) data were collected at an electrochemical workstation (CHI 660E, CH Instrumenets). CV curves were carried out at the scan rate of 0.1 mV s^{-1} between 3.0 and 4.6 V (*vs*. Li/Li^+). EIS were measured with a voltage of 5 mV amplitude in the frequency range of 100 kHz to 0.01 Hz, and carried out in a self-made three-electrode electrochemical cell with lithium metal as counter and reference electrodes.

Results and discussion

Structure and morphology characterizations

The XRD patterns of NCM622 coated with Al, Si and Ti oxides are compared with those of pristine NCM622, respectively. As shown in Figure 2, XRD patterns of all samples are in good accordance with a hexagonal α-$NaFeO_2$ layered structure belonging to the R-3m space group, and no obvious impurities and secondary phase are observed.

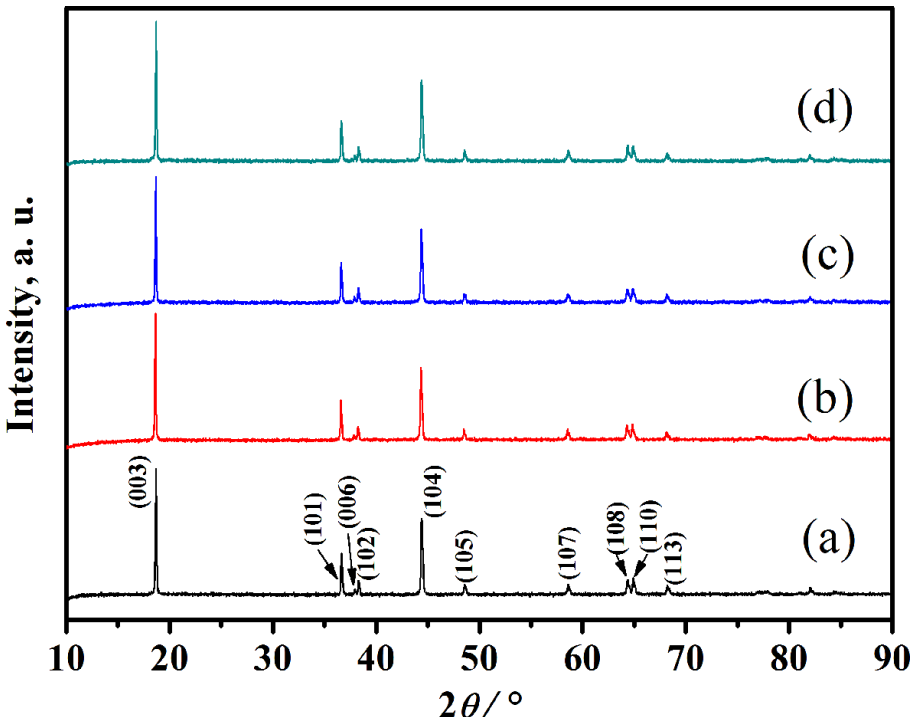

Figure 2. *XRD patterns of* ***(a)*** *P-NCM622,* ***(b)*** *A-NCM622,* ***(c)*** *S-NCM622 and* ***(d)*** *T-NCM622.*

Besides, the well-defined doublets of 006/102 and 108/110 for all samples indicate that these materials have a well-developed layered structure [29-31]. For three oxide-coated NCM622 samples, however, there is no diffraction peaks of Al_2O_3, SiO_2 and TiO_2 observed in each XRD pattern, which may be attributed to low amount of oxide existing on the surface of NCM622.Moreover, crystal lattice parameters listed in Table 1 were calculated from XRD patterns mentioned above. As

is seen in Table 1, XRD patterns of three oxide-coated particles show no significant changes in a and c lattice parameters and their c/a ratios, suggesting that the crystal structure of NCM622 is not affected by each oxide coating.

Table 1. *Lattice parameters, c/a and I(003)/I(104) values of samples.*

Sample	Lattice parameters, Å		c/a	$I_{(003)}/I_{(104)}$
	a	c		
P-NCM622	2.8711	14.2248	4.9545	1.31
A-NCM622	2.8738	14.2404	4.9553	1.37
S-NCM622	2.8725	14.2324	4.9547	1.35
T-NCM622	2.8725	14.2197	4.9503	1.32

Morphology of all samples is characterized by SEM, and the images are shown in Figure 3. It can be seen that particles of all samples present irregular spherical shapes, and particle sizes remained unchanged after surface modifications with different oxides.

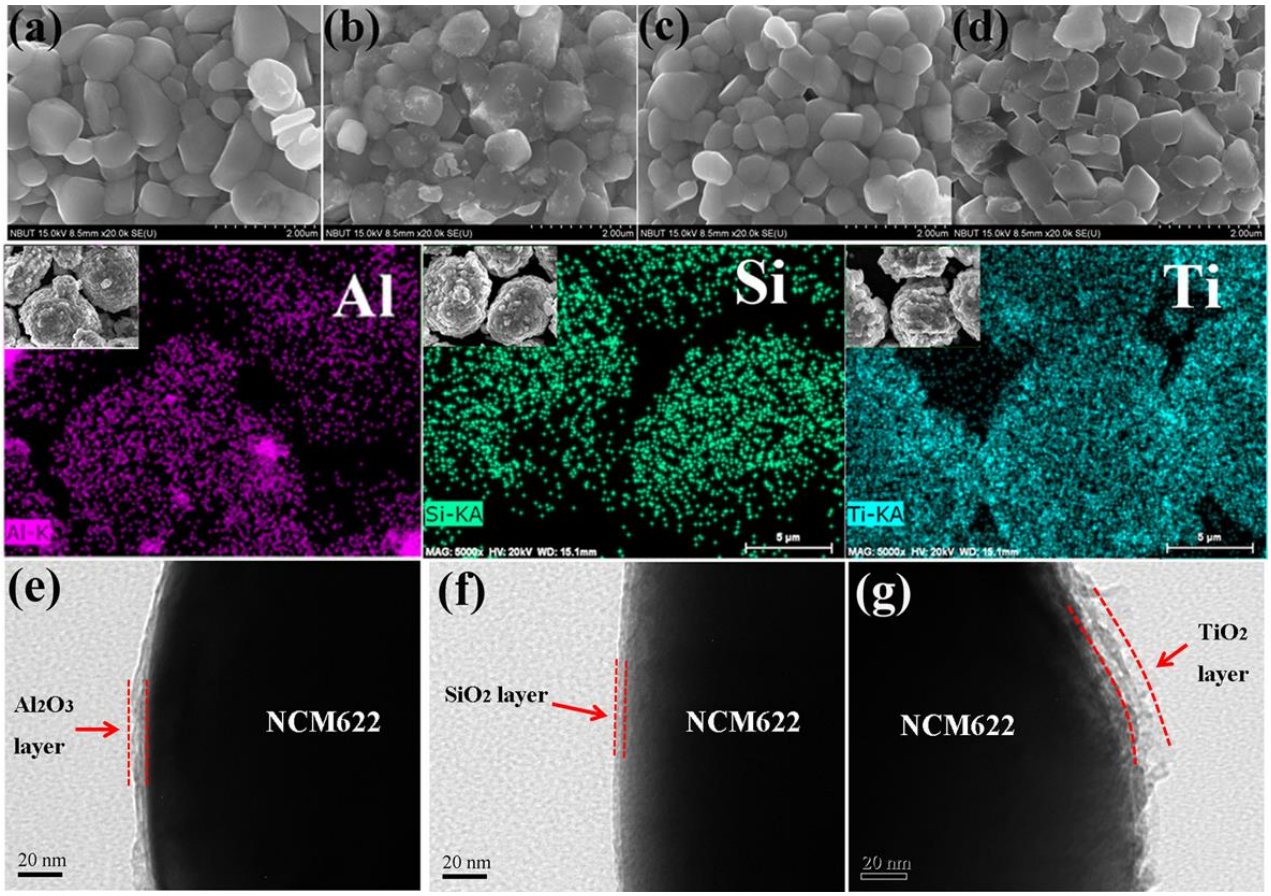

Figure 3. *SEM, TEM and corresponding EDS-mapping results:* ***(a)*** *P-NCM622;* ***(b,e)*** *A-NCM622;* ***(c,f)*** *S-NCM622;* ***(d,g)*** *T-NCM622 samples.*

Moreover, as shown in Figure 3a, the surface of pristine NCM622 is relatively smooth and seems rather "clean". For three oxide-coated NCM622 samples, however, there is an obvious difference in the surface morphology. As shown in Figure 3b, many small particles are attached on the surface of NCM622, forming a small number of Al agglomerates. Similarly, the surface of TiO_2-coated NCM622 is coated by some small particles and becomes rough (Fig. 3d). As seen from Figure 3c, the surface of SiO_2-coated NCM622 reveals no distinguishable difference compared with the rather smooth pristine NCM622.Additionally, EDS mapping has been carried out to identify the elements on the

surface of oxide-coated NCM622 particles. As shown in the middle part of Figure 3, homogeneous distributions of Al, Si and Ti are observed for the oxide-coated NCM622.All coatings covered the whole surface homogeneously, proving that all oxides coating layers are successfully formed on the surface of NCM622 material. Figures 3e-g present TEM images of three oxide-coated samples, where it can be seen that in each case, a complete thin oxide layer with a 5-10 nm thickness is formed on the surface of sample. For TiO_2 coating, however, a thin floc-like layer which makes the morphology different than that of SiO_2 and Al_2O_3 coatings can be noticed in Figure 3g. The surface differences among three distinct oxide coatings may give rise to different electrochemical performances of the coated NCM622.

Electrochemical characteristics

To investigate the influence of oxide coating layer on the electrochemical performance of NCM622 cathode material, three oxide-coated samples and pristine counterpart cells with Li anodes were tested by galvanostatic charging/discharging at 0.1 and 1 C (1 C = 160 mA g^{-1}) in the voltage range of 3.0-4.4 V, at different temperatures (25 and 50 °C).

Figure 4a illustrates the initial charge/discharge curves measured at 0.1 C, where the discharge capacity of the pristine sample is 191 mAh g^{-1}. The initial discharge curve of Al_2O_3-coated NCM622 is basically identical with that of the pristine sample, and the discharge capacity is also about 191 mAh g^{-1}.For SiO_2 and TiO_2 coatings, however, initial discharge capacities are slightly decreased to about 180 and 177 mAh g^{-1}, respectively. As shown in Figure 4b, the initial coulombic efficiency does not change much after oxide coatings.

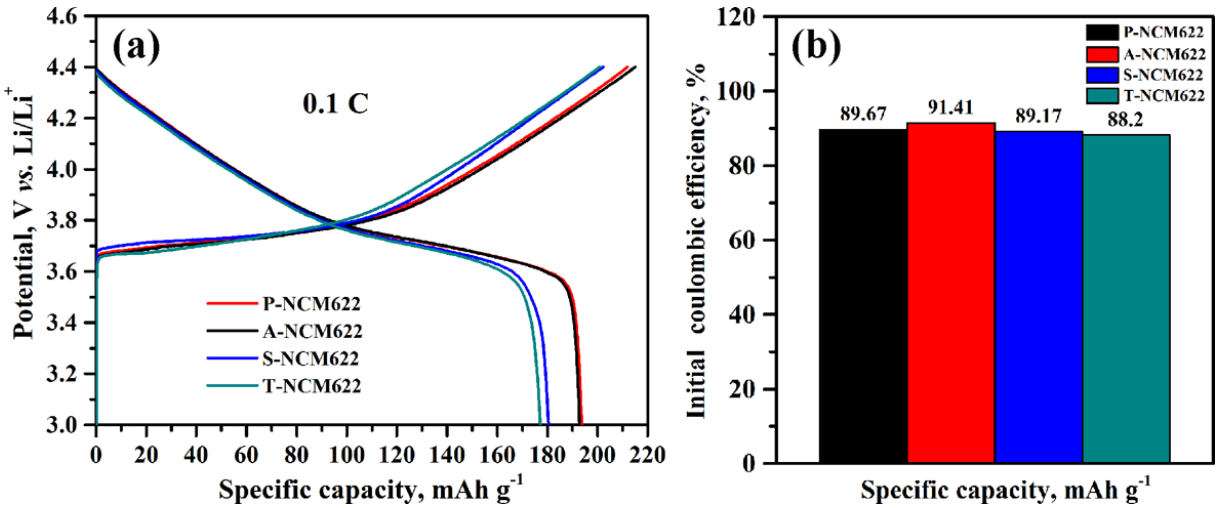

Figure 4. (a) *Initial charge-discharge curves of all samples in the voltage range of 3.0-4.4 V at 0.1 C.* ***(b)*** *the corresponding initial coulombic efficiency.*

Figures 5a and 5c depict initial charge/discharge curves measured at different temperatures (25 and 50 °C) at 1 C, showing almost the same phenomena as in Figure 4. Differences between initial discharge capacities may be related to the surface morphology of NCM622 and the properties of each oxide itself what could result in different resistances to Li ion migration or electron transfer in three oxide coating layers and lead to diverse electrochemical performance. Compared with other oxide coatings, it seems that Al_2O_3 coating layer formed on the surface of NCM622 is the most favorable for Li ion transport and electron transfer.

Figures 5b and 5d reveal changes in cycle performance for three oxide-coated samples, performed between 3.0 and 4.4 V at 1 C and high and low temperatures, respectively. Under the test condition of 25 °C, the discharge capacity of pristine NCM622 is weakly decreased during

cycling, and the initial discharge capacity and capacity retention ratio of pristine sample are 177 mAh g^{-1} and 94 %, respectively (shown also in Table 2). When the test temperature increased to 50 °C, however, the capacity retention ratio dramatically decreased to 70 %, *i. e.* the capacity retention ratio is reduced by 24 %.

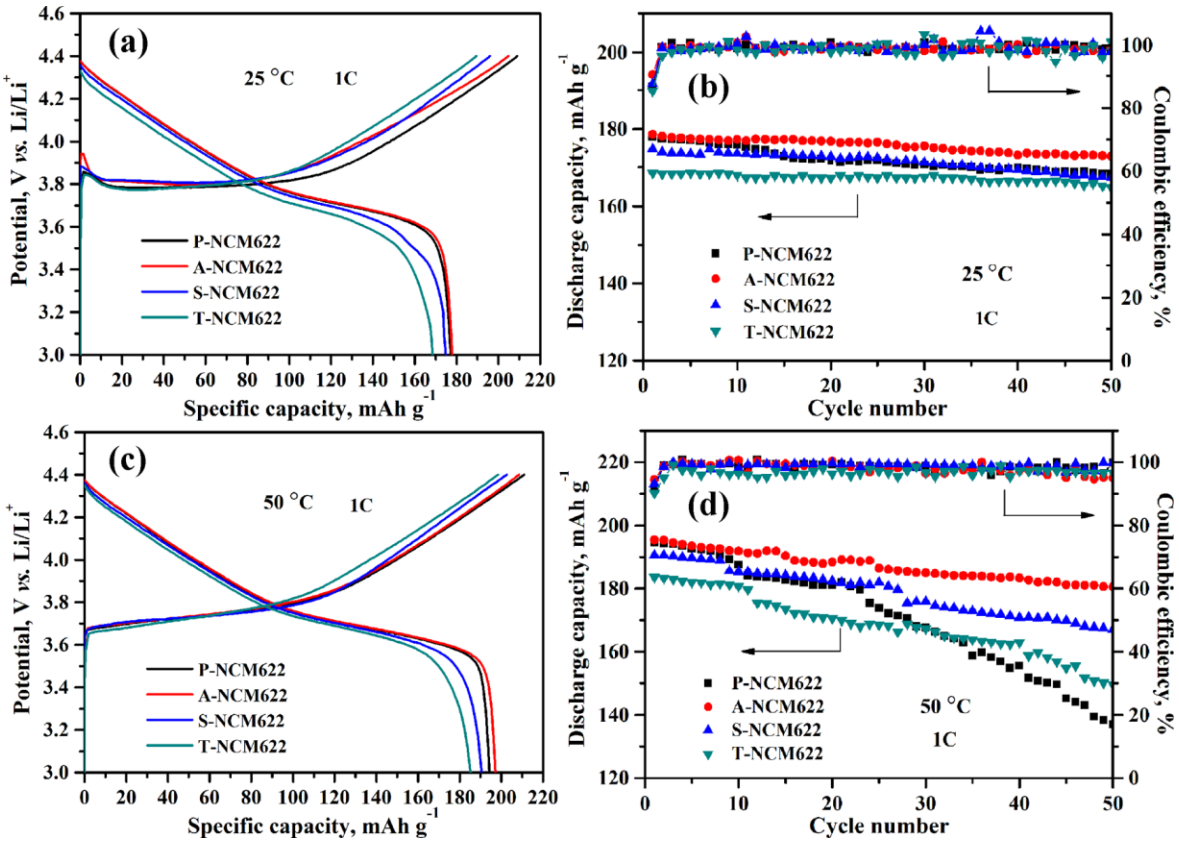

Figure 5. *Initial charge-discharge curves of all samples in the voltage range of 3.0-4.4 V at 1 C at different temperatures* ***(a)****: 25 °C,* ***(c)****: 50 °C. Cycle performance curves of all samples at* ***(b)****: 25 °C,* ***(d)****: 50 °C.*

The appearance of deterioration phenomenon may be attributed to high temperature aggravation of the side reactions between the cathode surface and the electrolyte and the structural damage of NCM622 during charge-discharge cycling, which will hinder Li ion migration and thus reduce the cycle stability. In comparison with the pristine one, the oxide-coated samples display capacity retention rates of 96, 95 and 97 % for A-NCM622, S-NCM622 and T-NCM622 after 50 cycles at 25 °C (Fig. 5b), which shows similar curve trends with the pristine sample. That is to say, at low temperature, the oxide coating effect is not conspicuous after repeated charge-discharge cycling. However, at high temperature, the cycle performance of oxide coated-samples is largely enhanced related to the pristine electrode (Fig. 5d). Moreover, data listed in Table 2 indicate that when the temperature increased from 25 to 50 °C, the reduction of capacity retention ratios for oxide coated samples is less than of the pristine one. This suggests that oxide coating could restrain the cycle deterioration at high temperature. Especially, for A-NCM622 sample, the reduction of capacity retention ratio is only 4 %, which is less than for other two samples. It seems that under the condition of high temperature cycling, the Al_2O_3 coating layer could better inhibit side reactions between electrode and electrolyte and thus show its superiority among all oxide-coated samples treated here.

Figure 6 exhibits the rate capabilities of all samples at various discharging rates performed between 3.0 and 4.4 V.

Table 2. *Electrochemical performance of lithium-ion cells with P-NCM622, A-NCM622, S-NCM622 and T-NCM622 at different temperatures after 50 cycles between 3.0 and 4.4 V at 1 C.*

	Sample	Capacity, mAh g^{-1}			
		P- NCM622	A- NCM622	S- NCM622	T- NCM622
25 °C	Initial discharge capacity	177	178	174	168
	Capacity retention, %	94	96	95	97
50 °C	Initial discharge capacity	194	195	190	183
	Capacity retention, %	70	92	87	81
25→50 °C	Reduction of retention, %	24	4	8	16

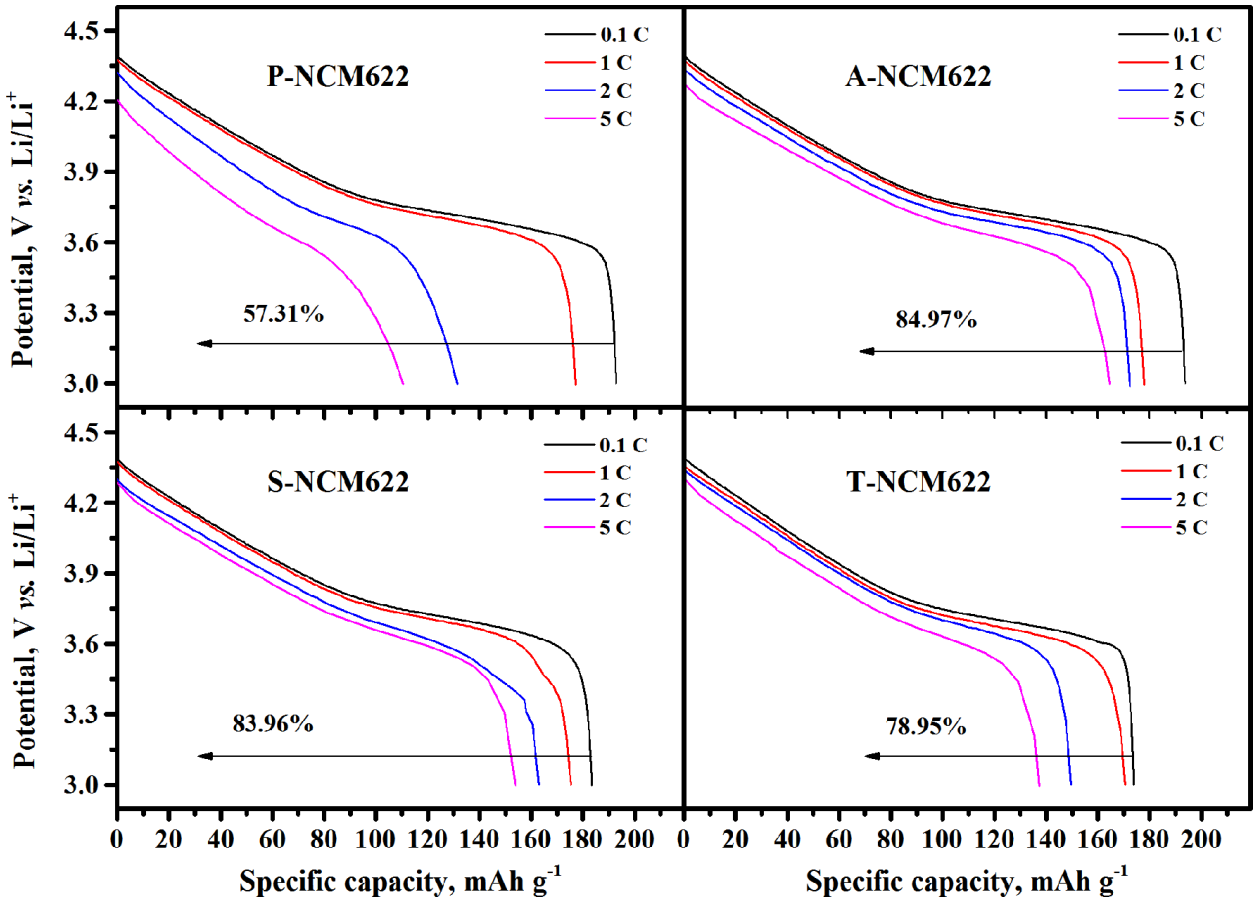

Figure 6. *Discharge rate performance of all samples.*

As seen from Figure 6, as the current density increased (from 0.1 C to 5 C), the discharge capacity of pristine sample decreased rapidly, and its capacity retention is only 57.31 %. The distinct decrease in discharge capacity of pristine NCM622 sample may be due to the slow kinetics at high rates, and destruction of the surface resulting from the side reactions between the active material and electrolyte. In contrast, after oxide coatings, the capacity retention increased to about 80 %, which shows better rate capability. Compared with S-NCM622 and T-NCM622 samples, A-NCM622 electrode delivered the highest discharge capacity of 191 mAh g^{-1} at 0.1 C, and still has capacity retention of 84.97 % when the cell was discharged at 5 C.

In order to better elucidate the possible role of oxide coating, the cycle stability of NCM622 material at high cutoff voltage is measured at the rate of 1 C. As shown in Figure 7a, when the charge cutoff voltage increased to 4.6 V, the capacity retention rate of the pristine sample dropped dramatically, retaining only 41 % after 50 cycles. This is attributed to the cation dissolution into electrolyte and interfacial reaction, what is schematically sketched in Figure 7b.

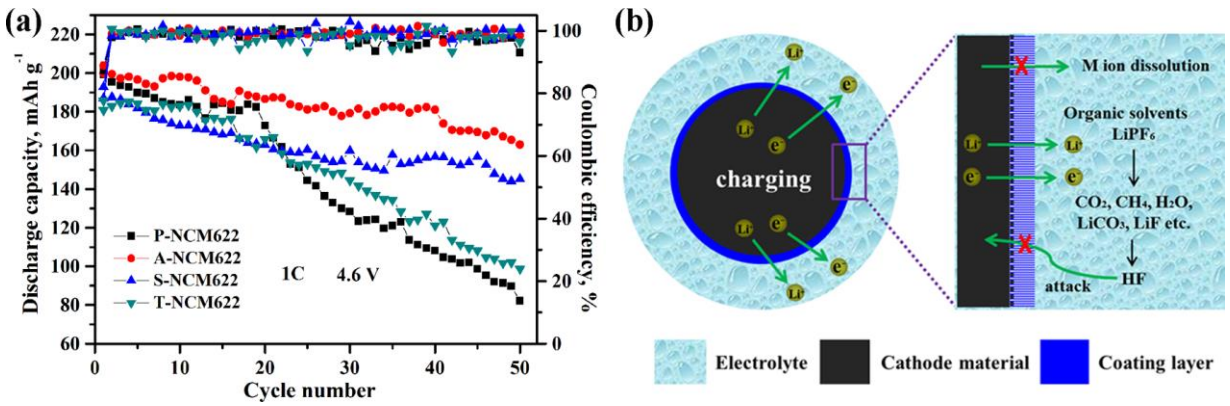

Figure 7. (a) *Cycle performance curves of all samples between 3.0 and 4.6 V at 1 C.* ***(b)*** *Schematic diagram of interfacial reactions between electrode and electrolyte.*

High cutoff voltage will aggravate decomposition of organic solvents and further promote mutual reaction between electrode and electrolyte. Also, as the charge-discharge cycle increases, more transition metal ions may dissolute into electrolyte and the attack action of HF generated in electrolyte during cycling could be more prominent. For three different oxide coating samples, however, the downward trend is also different. Compared with S-NCM622 and T-NCM622 samples, A-NCM622 sample showed excellent capacity retention, which still retained 81 % in the voltage range from 3.0 to 4.6 V. Besides, under different charge cutoff voltages, the specific capacity of A-NCM622 sample is also higher than of other samples. As the charge cutoff voltage increased from 4.4 V to 4.6 V, this gap becomes obviously wide.

Cycling performances of A-NCM622 sample described in the present report and few earlier reports on oxide-coated $LiNi_{0.6}Co_{0.2}Mn_{0.2}O_2$ electrodes are compared in Table 3. Some differences observed among different literature data can be connected with different oxide coating layers that are strongly related to unique chemical and physical properties of each oxide itself [38]. Therefore, after coating with different oxides, the cycle life of the cathode material can be extended diversely.

Table 3. *Cycling performance of different oxides coated $LiNi_{0.6}Co_{0.2}Mn_{0.2}O_2$ electrodes*

Cathodes and reference	Coating material	Cycling rate, C / cutoff voltage, V	Initial discharge capacity, mAh g^{-1}	Capacity retention ratio, %	Surface loading, mg cm^{-2}
NCM622 (this article)	Al_2O_3	1.0 /3.0-4.4	178	96 (50 cycles)	7-8
NCM622 [32]	Al_2O_3	1.0 /3.0-4.3	164	95 (30 cycles)	2-3
NCM622 [33]	SiO_2	0.5 / 3.0-4.3	165	95 (50 cycles)	2-3
NCM622 [34]	TiO_2	1.0 / 2.5-4.3	163	85 (100 cycles)	2-3
NCM622 [35]	TiO_2	1.0 / 3.0-4.5	177	88 (50 cycles)	2-3
NCM622 [36]	Co_3O_4	1.0 / 2.8-4.6	189	60 (100 cycles)	2-3
NCM622 [37]	ZrO_2	0.1 / 2.8-4.3	174	83 (100 cycles)	4

To further explore possible reasons of different electrochemical performances observed for three different oxide-NCM622 samples, EIS tests were performed after initial cycle performed between 3.0 and 4.4 V at 1 C. As shown in Figure 8, all impedance curves presented as Nyquist plots (Z'' *vs.* Z') can be distinguished in two sections. Depressed semicircle responses are observed in higher frequency region, while sloping line responses are observed in lower frequency region, respectively. Diameter of a semicircle can be regarded as the charge transfer resistance value (R_{ct}), which is an important parameter determining the difficulty of charge transfer [39-41]. And the *CPE* represents the

corresponding constant phase element. The impedance parameters are calculated by the simplified electrical equivalent circuit (EEC) shown in Figure 8a.

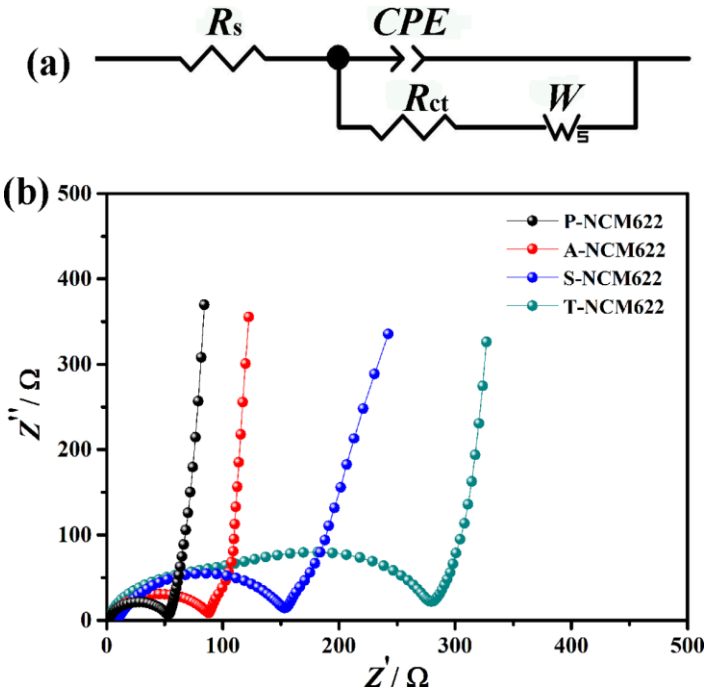

Figure 8. *(a) EEC performed to fit (b) Nyquist plots of P-NCM622, A-NCM622, S-NCM622 and T-NCM622 after initial cycle between 3.0 and 4.4 V at 1 C.*

In Table 4, the calculated values of resistive impedance parameters R_{ct} and R_s are listed, where R_s is resistance at the highest frequency, determined mostly by the electrolyte solution resistance. Apparently, the charge transfer resistance value of pristine sample is 52.8 Ω, while after coating with oxides, charge transfer resistance values become higher, attaining values of, 83.9, 151.8 and 278.6 Ω for A-NCM622, S-NCM622 and T-NCM622, respectively.

Table 4. *Resistive impedance parameter values obtained by fitting of EEC in Fig. 8a to impedance spectra in Fig. 8b*

sample	P-NCM622	A-NCM622	S-NCM622	T-NCM622
R_s / Ω	3.3	4.7	12.6	3.9
R_{ct} / Ω)	52.8	83.9	151.8	278.6

This phenomenon could be attributed to the inactive oxide layers, which may be subjected to diffusion limitation and thus to an increase of impedance. Additionally, the value of R_{ct} for A-NCM622 samples is the smallest among all coated samples, which may be more beneficial to Li^+ insertion/extraction compared with other two oxide-coated samples.

To better understand the effect of three different oxide coating layers on electrochemical properties in the charge-discharge processes, the cyclic voltammetry curves of all samples were additionally measured. As shown in Figure 9, a pair of sharp redox peaks is observed within 3.6-4.0 V, which is related to the oxidation and reduction reactions between Ni^{2+}/Ni^{3+} and Ni^{4+} [42]. Besides, there is only one pair of redox peaks appeared in the first five cycles, which suggest that the phase transition from hexagonal to monoclinic is not taking place at 3.0-4.6 V, and the oxide coating layer has no negative effect on the electrochemical reaction.

According to the relevant literature [43,44], the magnitude of the potential gap between the anodic and cathodic peak (Δv) can be used to qualitatively describe the reversibility/polarization of the electrochemical process. The potential gap values (0.069, 0.128 and 0.198 V) of redox peaks for

three coated NCM622 samples are considerably smaller than those of the pristine sample (0.280 V), indicating that the interfacial polarization of cathode is inhibited by oxide coating. Al_2O_3-coated NCM622 electrode exhibits the lowest potential gap, thereby obtaining the lowest polarization.

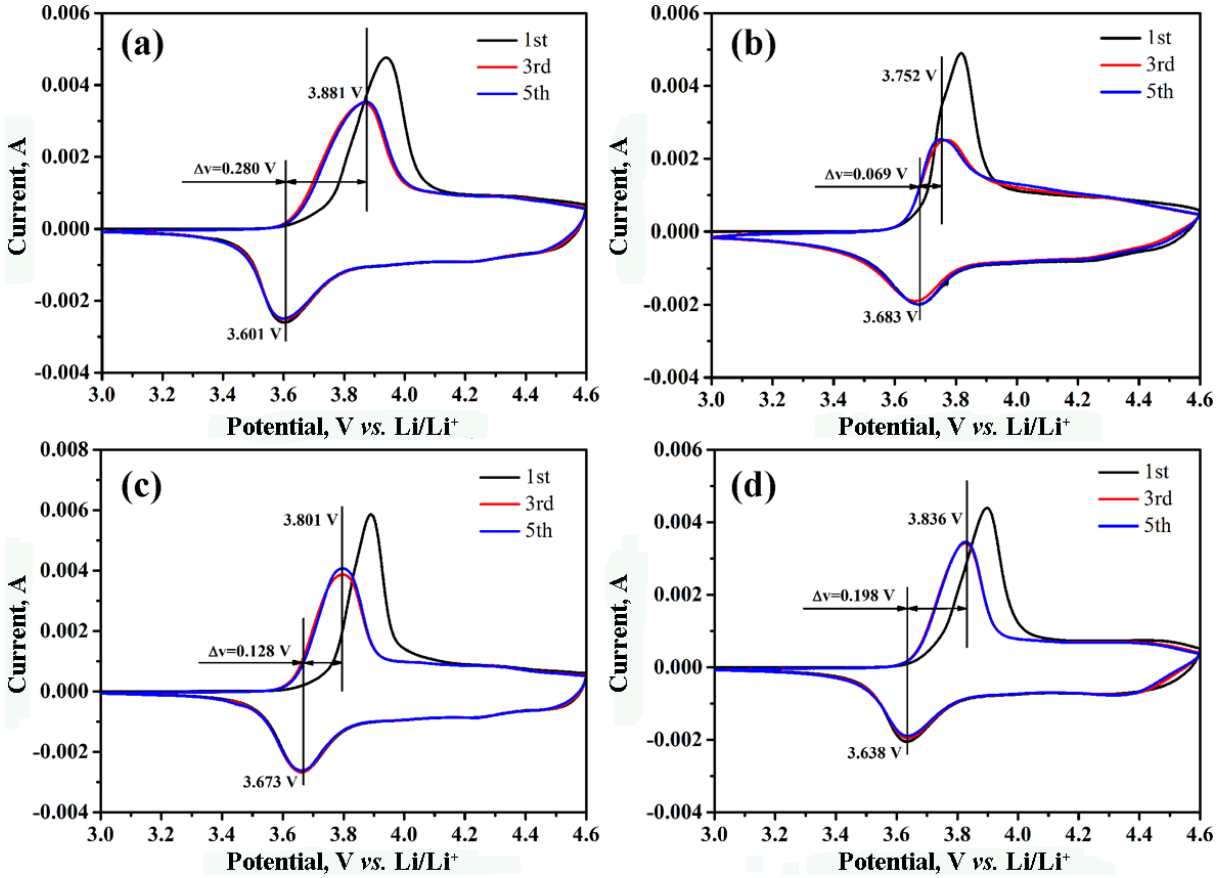

Figure 9. *CV curves at scan rate of 0.1 mV $s^{-1}$of* ***(a)*** *P-NCM622,* ***(b)*** *A-NCM622,* ***(c)*** *S-NCM622 and* ***(d)*** *T-NCM622.*

This suggests that reversibility of the Al_2O_3-coated electrode is the best among all sample electrodes. Therefore, CV results clearly demonstrated that lower polarization and better reversibility of Li ions insertion/de-insertion for Al_2O_3 coating sample can be achieved, which is well in line with its superior electrochemical properties.

Conclusions

In this paper, oxide coating layers of Al, Si and Ti were successfully prepared on the surface of $LiNi_{0.6}Co_{0.2}Mn_{0.2}O_2$ (NCM622) electrode by the hydrolysis coating technology. The relationship between the kind of oxide coating layer and electrochemical behavior of coated NCM622 electrode was investigated. Electrochemical measurements demonstrated that compared with SiO_2 and TiO_2-coated samples, NCM622 electrode coated with Al_2O_3 layer exhibited higher discharge capacity and better cycle stability. It was also found that cycle stability of this electrode can be significantly improved at increased test temperature and cutoff voltage. The improved electrochemical performance of Al_2O_3 coated electrode is mainly attributed to the suppression of mutual reaction between electrode and electrolyte. Thus, as the charge-discharge cycle increases, the dissolution of some transition metal ions may be restrained by the Al_2O_3 coating layer. Additionally, it was shown that Al_2O_3 coating layer could better decrease the polarization gap accompanying the charge-discharge processes and achieve better reversibility of Li ions intercalation/deintercalation. The

obtained results suggest that Al_2O_3 modification of the surface by this convenient method may play a promoting role for application of NCM622 cathode material in lithium ion batteries.

Acknowledgements: *This research was supported by National Natural Science Foundation of China (NO. 51571168), the National Key R&D Program of China (NO. 2016YFB0701401), and the Ministry of Science and Technology of China (No. 2014DFA53040).*

References

[1] D. Larcher, J. M. Tarascon, *Nature Chemistry* **7** (2015) 19-29.
[2] G. L. Soloveichik, *Annual Review of Chemical and Biomolecular Engineering* **2** (2011) 503-27.
[3] P. G. Bruce, S. A. Freunberger, L. J. Hardwick, J. M. Tarascon, *Nature Materials* **11** (2012) 19-29.
[4] B. Dunn, H. Kamath, J. M. Tarascon, *Science* **334** (2011) 928-935.
[5] X. He, C. Du, B. Shen, C. Chen, X. Xu, Y. Wang, P. Zuo, Y. Ma, X. Cheng, G. Yin, *Electrochimica Acta* **236** (2017) 273-279.
[6] J. Duan, G. Hu, Y. Cao, C. Tan, C. Wu, K. Du, Z. Peng, *Journal of Power Sources* **326** (2016) 322-330.
[7] L. Li, Q. Yao, H. Zhu, Z. Chen, L. Song, J. Duan, *Journal of Alloys and Compounds* **686** (2016) 30-37.
[8] Y. Zeng, K. Qiu, Z. Yang, F. Zhou, L. Xia, Y. Bu, *Ceramics International* **42** (2016) 10433-10438.
[9] Y. Kobayashi, M. Tabuchi, H. Miyashiro, N. Kuriyama, *Journal of Power Sources* **364** (2017) 156-162.
[10] J. Zhang, Z. Yang, R. Gao, L. Gu, Z. Hu, X. Liu, *ACS Applied Materials & Interfaces* **9** (2017) 29794-29803.
[11] J. L. Shi, J. N. Zhang, M. He, X. D. Zhang, Y. X. Yin, H. Li, Y. G. Guo, L. Gu, L. J. Wan, *ACS Applied Materials & Interfaces* **8** (2016) 20138-20146.
[12] X. Xiong, D. Ding, Z. Wang, B. Huang, H. Guo, X. Li, *Journal of Solid State Electrochemistry* **18** (2014) 2619-2624.
[13] B. Zhang, P. Dong, H. Tong, Y. Yao, J. Zheng, W. Yu, J. Zhang, D. Chu, *Journal of Alloys and Compounds* **706** (2017) 198-204.
[14] G. Hu, M. Zhang, L. Wu, Z. Peng, K. Du, Y. Cao, *Journal of Alloys and Compounds* **690** (2017) 589-597.
[15] H. Wu, Z. Wang, S. Liu, L. Zhang, Y. Zhang, *ChemElectroChem* **2** (2015) 1921-1928.
[16] S. S. Jan, S. Nurgul, X. Shi, H. Xia, H. Pang, *Electrochimica Acta* **149** (2014) 86-93.
[17] D. Zuo, G. Tian, D. Chen, H. Shen, C. Lv, K. Shu, Y. Zhou, *Electrochimica Acta* **178** (2015) 447-457.
[18] L. Li, M. Xu, Q. Yao, Z. Chen, L. Song, Z. Zhang, C. Gao, P. Wang, Z. Yu, Y. Lai, *ACS Applied Materials & Interfaces* **8** (2016) 30879-30889.
[19] S. Chen, T. He, Y. Su, Y. Lu, L. Bao, L. Chen, Q. Zhang, J. Wang, R. Chen, F. Wu, *ACS Applied Materials & Interfaces* **9** (2017) 29732-29743.
[20] H. Yu, S. Qian, L. Yan, P. Li, X. Lin, M. Luo, N. Long, M. Shui, J. Shu, *Journal of Alloys and Compounds* **667** (2016) 58-64.
[21] Y. Uchimoto, H. Sawada, T. Yao, *Journal of Power Sources* **97-98** (2001) 326-327.
[22] M. Dong, Z. Wang, H. Li, H. Guo, X. Li, K. Shih, J. Wang, *ACS Sustainable Chemistry & Engineering* **5** (2017) 10199-10205.
[23] J. Z. Kong, S. S. Wang, G. A. Tai, L. Zhu, L. G. Wang, H. F. Zhai, D. Wu, A. D. Li, H. Li, *Journal of Alloys and Compounds* **657** (2016) 593-600.
[24] W. Luo, B. Zheng, *Applied Surface Science* **404** (2017) 310-317.
[25] J. Z. Kong, C. Ren, G. A. Tai, X. Zhang, A. D. Li, D. Wu, H. Li, F. Zhou, *Journal of Power Sources* **266** (2014) 433-439.
[26] H. Cao, B. Xia, Y. Zhang, N. Xu, *Solid State Ionics* **176** (2005) 911-914.
[27] N. Ariel, G. Ceder, D. R. Sadoway, E. A. Fitzgerald, *Journal of Applied Physics* **98** (2005) 023516-023516-7.
[28] H. M. Cheng, F. M. Wang, J. P. Chu, R. Santhanam, J. Rick, S. C. Lo, *Journal of Physical Chemistry C* **116** (2012) 7629-7637.
[29] S. Liu, H. Wu, L. Huang, M. Xiang, H. Liu, Y. Zhang, *Journal of Alloys and Compounds* **674** (2016) 447-454.
[30] L. Liang, F. Jiang, Y. Cao, G. Hu, K. Du, Z. Peng, *Journal of Power Sources* **328** (2016) 422-432.

[31] F. Wu, J. Tian, Y. Su, J. Wang, C. Zhang, L. Bao, T. He, J. Li, S. Chen, *ACS Applied Materials & Interfaces* **7** (2015) 7702-7708.
[32] Y. Chen, Y. Zhang, F. Wang, Z. Wang, Q. Zhang, *Journal of Alloys and Compounds* **611** (2014)135-141.
[33] W. Cho, S. M. Kim, J. H. Song, T. Yim, S. G. Woo, K. W. Lee, J. S. Kim, Y. J. Kim, *Journal of Power Sources* **282** (2015) 45-50.
[34] C. C. Qin, J. L. Cao, J. Chen, G. L. Dai, T. F. Wu, Y. Chen, Y. F. Tang, A. D. Li, Y. Chen, *Dalton Transactions* **45** (2016) 9669-9675.
[35] Y. Chen, Y. Zhang, B. Chen, Z. Wang, C. Lu, *Journal of Power Sources* **256** (2014) 20-27.
[36] F. Tao, X. X. Yan, J. J. Liu, H. L. Zhang, L. Chen, *Electrochimica Acta* **210** (2016) 548-556.
[37] T. Tao, C. Chen, Y. Yao, B. Liang, S. Lu, Y. Chen, *Ceramics International* **43** (2017) 15173-15178.
[38] D. Zuo, G. Tian, X. Li, D. Chen, K. Shu, *Journal of Alloys and Compounds* **706** (2017) 24-40.
[39] Y. Q. Lai, M. Xu, Z. A. Zhang, C. H. Gao, P. Wang, Z. Y. Yu, *Journal of Power Sources* **309** (2016)20-26.
[40] J. Duan, C. Wu, Y. Cao, K. Du, Z. Peng, G. Hu, *Electrochimica Acta* **221** (2016) 14-22.
[41] E. Zhao, M. Chen, Z. Hu, D. Chen, L. Yang, X. Xiao, *Journal of Power Sources* **343** (2017) 345-353.
[42] D. Wang, X. Li, Z. Wang, H. Guo, X. Chen, X. Zheng, Y. Xu, J. Ru, *Electrochimica Acta* **174** (2015) 1225-1233.
[43] K. Liu, G. L. Yang, Y. Dong, T. Shi, L. Chen, *Journal of Power Sources* **281** (2015) 370-377.
[44] D. Wang, X. Li, Z. Wang, H. Guo, Z. Huang, L. Kong, J. Ru, *Journal of Alloys and Compounds* **647** (2015) 612-619.